

SKIFFS: Superconducting Kinetic Inductance Field-Frequency Sensors for Sensitive Magnetometry in Moderate Background Magnetic Fields

A. T. Asfaw,^{1, a)} E. I. Kleinbaum,¹ T. M. Hazard,¹ A. Gyenis,¹ A. A. Houck,¹ and S. A. Lyon¹
Department of Electrical Engineering, Princeton University, Princeton, New Jersey 08544, USA

(Dated: 12 October 2018)

We describe sensitive magnetometry using lumped-element resonators fabricated from a superconducting thin film of NbTiN. Taking advantage of the large kinetic inductance of the superconductor, we demonstrate a continuous resonance frequency shift of 27 MHz for a change in magnetic field of $1.8 \mu\text{T}$ within a perpendicular background field of 60 mT. By using phase-sensitive readout of microwaves transmitted through the sensors, we measure phase shifts in real time with a sensitivity of 1 degree/nT. We present measurements of the noise spectral density of the sensors, and find their field sensitivity is at least within one to two orders of magnitude of superconducting quantum interference devices operating with zero background field. Our superconducting kinetic inductance field-frequency sensors enable real-time magnetometry in the presence of moderate perpendicular background fields up to at least 0.2 T. Applications for our sensors include the stabilization of magnetic fields in long coherence electron spin resonance measurements and quantum computation.

Disordered superconductors such as NbTiN, TiN and NbN have become ubiquitous in several fields of study due to their large kinetic inductance and resilience to large background magnetic fields^{1,2}. Microwave kinetic inductance detectors³⁻⁵ and superconducting nanowire single-photon detectors^{6,7} fabricated from kinetic inductors are now routinely used in astronomy and imaging. Kinetic inductors can also be used in applications such as current-sensing⁸, magnetometry⁹, parametric amplification^{10,11}, generation of frequency combs¹², and superconducting qubits^{13,14}.

In this work, we take advantage of the kinetic inductance of a thin film of NbTiN to fabricate lumped-element resonators whose resonance frequencies are strongly dependent on the perpendicular magnetic field, changing by as much as 27 MHz for a field change of $1.8 \mu\text{T}$. We demonstrate a method for real-time measurement of AC magnetic fields based on phase-sensitive readout of microwave transmission through the resonators, finding a detection sensitivity of 1 degree/nT. Our Superconducting Kinetic Inductance Field-Frequency Sensors (SKIFFS) are able to operate in perpendicular background magnetic fields at least as large as 0.2 T, and may find applications in quantum computation, where superconducting quantum interference devices (SQUIDs) based on Josephson junctions may not be applicable due to the large magnetic fields.

Our SKIFFS are fabricated from a 7 nm NbTiN thin film ($T_C \sim 9 \text{ K}$, $R_{\text{sheet}} = 252 \Omega/\square$) DC-sputtered reactively on a c-axis sapphire substrate using a NbTi alloy target and an Ar/N environment¹⁵. The device features are patterned using electron-beam lithography followed by reactive-ion etching with an SF_6/Ar plasma. A scanning electron micrograph of a SKIFFS is shown in figure Fig. 1a. The sensor is a lumped-element microwave resonator fabricated from a $100 \mu\text{m} \times 100 \mu\text{m}$ rectangular

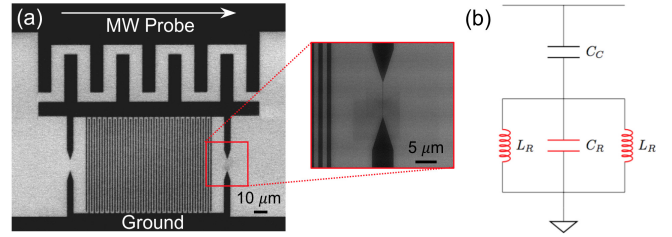


FIG. 1. (a) Scanning electron micrograph of a SKIFFS resonator. Each resonator consists of a $5 \mu\text{m}$ wide rectangular superconducting loop that is coupled to a central microwave feedline capacitively using four pairs of interdigitated $10 \mu\text{m}$ fingers. The loop inductance is mostly due to the two nanowires that are 100 nm wide as shown in the inset. Interdigitated capacitors with fingers of width $1 \mu\text{m}$ are placed at the center of the loop to complete the resonator, and the lower arm of the superconducting loop is shunted to ground. (b) Lumped-element circuit model of a SKIFFS resonator coupled to a microwave feedline via C_C . The kinetic inductors, L_R , on each arm of the superconducting loop and the capacitor, C_R , form the resonator.

superconducting loop defined by a $5 \mu\text{m}$ wide line. Two 100 nm wide nanowires of length ℓ_{nw} are defined on the left and right arms of the loop as seen in the inset of Fig. 1a. Care is taken to prevent current crowding at the ends of the nanowires^{16,17} by linearly tapering from the micron-wide loop dimensions to the nanowires over a length of $10 \mu\text{m}$. The resonator is completed by placing interdigitated capacitors at the center of the loop with fingers and gaps of width $1 \mu\text{m}$. Each resonator is coupled to a microwave feedline using a coupling capacitor, which is also an interdigitated structure with four pairs of $10 \mu\text{m}$ wide fingers that are separated by $10 \mu\text{m}$ gaps.

A lumped-element circuit model of the SKIFFS is shown in Fig. 1b. From a Sonnet¹⁸ simulation, we obtain an estimate of the resonator capacitance, $C_R \approx 0.2 \text{ pF}$. From the thin-film parameters, we estimate that the

^{a)}Electronic mail: asfaw@princeton.edu

nanowires contribute an inductance of $360 \text{ pH}/\mu\text{m}$, while the micron-sized sections of the loop contribute an inductance of $7.2 \text{ pH}/\mu\text{m}$. Using these parameters, we estimate a resonance frequency of 5 GHz for a sensor with $\ell_{\text{nw}} = 10 \mu\text{m}$.

The device reported in this work has six sensors with varying values of ℓ_{nw} from 7 to $12 \mu\text{m}$ that are coupled to a common microwave feedline. Following fabrication, the device is wirebonded to a copper printed circuit board equipped with microwave connectors and placed in the bore of an external magnet with the surface of the superconductor perpendicular to the magnetic field, B_0 . Additionally, a home-made Helmholtz pair coil is attached to the sample holder such that the generated field, B_{coil} , is parallel to the external field. We use the external magnet to generate the moderate background magnetic fields, and the coil to generate small additional magnetic fields. The magnetic field generated by the home-made coil was calibrated from the shift in the electron spin resonance line of phosphorus donor electron spins in silicon in a separate experiment.

The device and sample holder assembly are cooled to a temperature of 1.9 K , and microwave transmission through the central feedline is monitored using a network analyzer with a microwave power of -72 dBm at the device. All six resonances are found in the range of 3.945 to 5.230 GHz . Microwave powers exceeding -64 dBm were observed to distort the resonance lineshapes of some of the resonators. This behavior has been observed previously, and is a signature of the large kinetic inductance of the superconductor^{19,20}. For the remainder of this work, we focus on one of the SKIFFS with $\ell_{\text{nw}} = 10 \mu\text{m}$ and a resonance frequency near 4.2 GHz .

The loaded quality factor of the resonator depends strongly on the perpendicular magnetic field, B_0 . In order to study this dependence, we monitor the resonance near 4.2 GHz as B_0 is swept from 10 to 200 mT . The results are shown in Fig. 2a, where we have extracted the loaded quality factor as a function of the background magnetic field. As B_0 is increased, the quality factor drops from 1000 at $B_0 = 10 \text{ mT}$ to 200 at $B_0 = 200 \text{ mT}$. The inset shows microwave transmission through the device for $B_0 = 60 \text{ mT}$, producing a quality factor 600 . We remark here that the resonator is strongly overcoupled due to the choice of coupling capacitor parameters. A higher loaded quality factor at zero field can readily be obtained by adjusting the dimensions of the interdigitated capacitor coupling the resonator to the microwave feedline toward critical coupling. Additionally, higher quality factors should be possible by operating the resonator at lower temperatures, where $T/T_C \ll 0.1$. Quality factors between $10,000$ and $100,000$ have previously been reported for comparable thin films of NbTiN in the presence of moderate background fields at 300 mK ².

Next, we set $B_0 = 60 \text{ mT}$ and apply small magnetic fields using our home-made coil. The results are shown in Fig. 2b. As the magnetic field of the coil, B_{coil} , is increased, the resonance frequency, f_R , shifts continuously

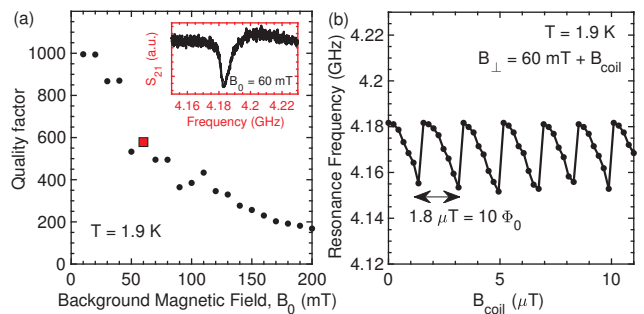


FIG. 2. (a) Quality factor of a SKIFFS resonator as a function of the perpendicular background magnetic field, B_0 . The inset shows microwave transmission through the device near one of the resonance frequencies at 4.182 GHz for $B_0 = 60 \text{ mT}$. (b) Shifts in the 4.182 GHz resonance frequency as a function of small field changes, B_{coil} , applied using a home-made Helmholtz pair coil. The perpendicular background magnetic field, B_0 , is 60 mT . The resonance frequency shifts by 27 MHz as B_{coil} changes by $1.8 \mu\text{T}$. The abrupt jump in the resonance frequency shift results from the finite screening current that can be supported by the superconducting loop at the thin nanowire sections, as described in the main text.

from its value at 60 mT as

$$\delta f_R(B_{\text{coil}}) = f_{R_0} \left(1 - \left(\frac{B_{\text{coil}}}{17 \mu\text{T}} \right)^2 \right) \quad (1)$$

where $f_{R_0} = 4.182 \text{ GHz}$ is the resonance frequency with $B_{\text{coil}} = 0 \mu\text{T}$ and $B_0 = 60 \text{ mT}$. The functional form of the shift in the resonance frequency has been observed in other devices^{1,9,21–23}. The resonance frequency shows a maximum shift of 27 MHz as B_{coil} is increased to $1.8 \mu\text{T}$. When B_{coil} exceeds $1.8 \mu\text{T}$ (~ 10 flux quanta), the resonance frequency abruptly jumps back to 4.182 GHz and continues to change as before. This behavior can be understood by noting that a screening current, i_{loop} , is generated in the superconducting loop in order to keep the magnetic flux threading the loop constant as B_{coil} is changed. This current modulates the kinetic inductance of the superconducting nanowires, L_R , thereby resulting in a change in the resonance frequency of the SKIFFS resonator. Eventually, as B_{coil} is increased, i_{loop} exceeds the critical current of the nanowires. From the data, we estimate the maximum i_{loop} to be $\sim 2 \mu\text{A}$. This results in the formation of a normal metal which breaks the superconducting loop, allowing additional magnetic flux to thread the loop as the normal section of the loop returns to the superconducting state. Once the loop returns to the superconducting state, there is no longer a screening current since there is no difference between the magnetic flux threading the loop and the applied magnetic flux due to B_{coil} .

Three observations support this interpretation of the abrupt jumps in f_R as B_{coil} is swept. The first is the functional form in Eq. 1, which is similar to the functional form of a kinetic inductor modulated by a DC current.

The screening current, i_{loop} , generated in the superconducting loop is related to the applied magnetic flux, B_{coil} , by the relation

$$i_{\text{loop}}L_{T_{\text{loop}}} - B_{\text{coil}}A_{\text{loop}} = n\Phi_0 \quad (2)$$

where $L_{T_{\text{loop}}}$ is the total loop inductance, A_{loop} is the loop area, Φ_0 is the magnetic flux quantum, and n is the integer number of flux quanta threading the superconducting loop⁹. The linear relationship between i_{loop} and B_{coil} provides an explanation for the similarity between the functional form of the change in resonance frequency, $\delta f_R(B_{\text{coil}})$, to the functional form of a kinetic inductor that is modulated by a DC current^{1,9,21–23}. Second, we have observed that the largest value of B_{coil} that can be screened before the abrupt jump occurs is strongly dependent on temperature, and is significantly reduced at higher temperatures. For instance, while $\sim 1.8 \mu\text{T}$ of magnetic field can be screened at a temperature of 1.9 K with a microwave power of -72 dBm, that value drops to only $\sim 1.2 \mu\text{T}$ at a temperature of 4.2 K. This observation supports our interpretation since the critical current of superconductors depends strongly on temperature for temperatures above $\sim 0.1T_C$ ²⁴. Third, we have also observed that higher microwave powers reduce the maximum B_{coil} that can be supported. This observation also supports our interpretation since larger microwave powers lead to larger microwave currents, which in turn limit the largest i_{loop} that can be supported in the nanowire. We note that similar abrupt jumps have been observed in the frequency of resonators tuned by nanoSQUIDs fabricated from Nb constrictions²⁵.

In order to demonstrate the application of SKIFFS for magnetometry, we use the experimental setup shown in Fig. 3a. A microwave probe tone is applied at the center of the SKIFFS resonance, f_R , and transmission through the device is monitored using phase-sensitive detection. An IQ mixer downconverts the microwave probe tone to DC such that the phase of microwave transmission through the device can be computed from its in-phase and quadrature components. For small changes in magnetic field, δB_{coil} , the phase of the microwave transmission, $\delta\phi$, follows linearly with a slope that depends on the quality factor of the resonator. We bias the SKIFFS with $B_{\text{coil}} \approx 1.3 \mu\text{T}$ such that the device sensitivity is $\sim 31 \text{ MHz}/\mu\text{T}$. Fig. 3b and c show the results of applying sinusoidal magnetic fields with amplitude of $\delta B_{\text{coil}} = 25 \text{ nT}$ peak-to-peak at a frequency of 1 kHz and 100 Hz, respectively. The phase of the transmitted microwaves shows oscillations which follow δB_{coil} . From the peak-to-peak change in the phase, we find a phase sensitivity of $\delta\phi/\delta B_{\text{coil}} \approx 1 \text{ degree}/\text{nT}$, in good agreement with an estimate of 0.9 degrees/nT from the independently measured quality factor of 600 and the bias point of $31 \text{ MHz}/\mu\text{T}$.

We estimate the noise of SKIFFS magnetometry by measuring their phase response to a small 500 Hz sinusoidal magnetic field. Next, we subtract the sinusoidal component from the measured phase response, and compute the power spectral density of the remaining noise.

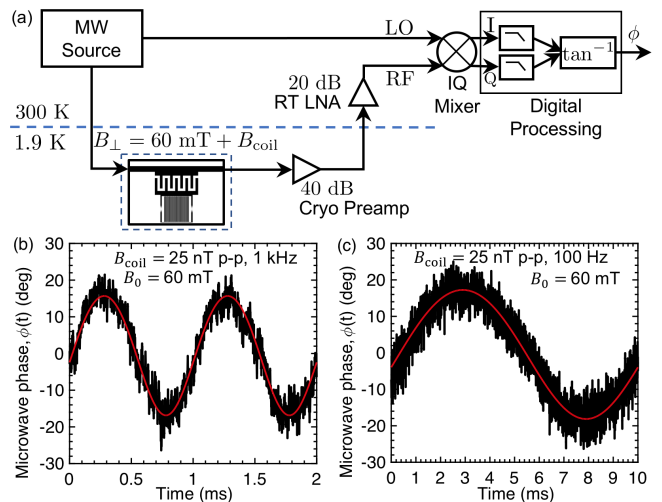


FIG. 3. (a) Measurement setup for real-time detection of small magnetic field fluctuations, δB_{coil} , using a SKIFFS resonator. Microwave transmission through the resonator is amplified and downconverted using an IQ mixer. The in-phase and quadrature outputs can be used to compute the phase of the transmitted microwaves. Changes in the microwave phase transmission are proportional to δB_{coil} . Parts (b) and (c) show the results of this computation for 25 nT peak-to-peak sinusoidal magnetic fields oscillating at 1 kHz and 100 Hz, respectively.

The results of this procedure are shown in Fig. 4 with and without a background magnetic field, B_0 , in addition to the sinusoidal excitation. For comparison, we have also included independent measurements of the magnetic field fluctuations in our experimental setup using dynamical decoupling noise spectroscopy^{26–29}, where the power spectral density is inferred from the phase accumulated due to magnetic field fluctuations present during an electron spin resonance experiment with phosphorus donor spins in silicon at 340 mT.

The square-root power spectral density is a factor of 2 larger in the presence of a background magnetic field, likely due in part to fluctuations in the external magnetic field and vibration-induced noise in our experimental setup. Measurements at both fields show $f^{-0.5}$ dependence, indicating the presence of $1/f$ noise power in the detection similar to low-temperature SQUIDs³⁰. The agreement between the magnetic field noise measured using SKIFFS and electron spins suggests that our measurement of the SKIFFS noise may be limited by fluctuations in the external magnetic field^{31,32}. Further work is necessary to separate the baseline noise of SKIFFS from the fluctuations in the external magnet.

The value of the power spectral density in Fig. 4 is $\sim 10 \text{ pT}/\sqrt{\text{Hz}}$ ($50 \mu\Phi_0/\sqrt{\text{Hz}}$) at 1 kHz, indicating that our devices are at worst one to two orders of magnitude more noisy than typical low-temperature SQUIDs at comparable frequencies in zero background field³³. Previous work^{34,35} has shown that two-level fluctuators can lead to a $1/f$ noise power which has a typical value of

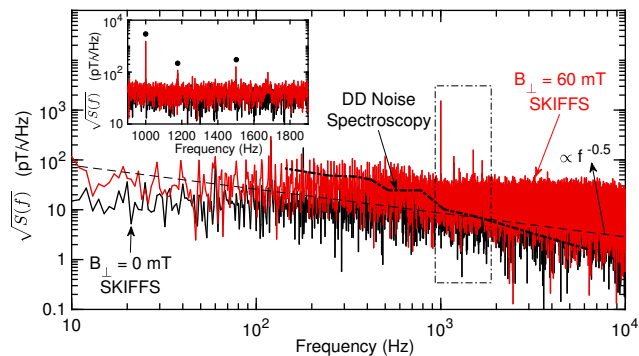


FIG. 4. Square-root noise power spectral density of a SKIFFS resonator, measured by computing the Fourier transform of the detected phase signal as described in the main text for the cases with and without a background perpendicular magnetic field. The dashed line shows a $f^{-0.5}$ fit, indicating that the noise power is of $1/f$ -type. The dash-dotted line shows a measurement of the fluctuations present in the external magnetic field using dynamical decoupling noise spectroscopy, indicating that our measurement of the SKIFFS noise is likely limited by fluctuations in the external magnet. The inset shows a zoom-in near 1 kHz, where spurious harmonics of the calibration signal from our waveform generator are apparent, as well as a previously characterized source of magnetic field fluctuations in our setup at 1.175 kHz.

$S_B^{1/2}(1 \text{ Hz}) = 1 \mu\Phi_0/\sqrt{\text{Hz}}$, indicating the potential for improved sensitivity of our devices by two orders of magnitude. Kinetic inductance magnetometry with a noise floor of $30 \text{ fT}/\sqrt{\text{Hz}}$ has previously been reported in a device fabricated from NbN and operated in a shielded environment with zero background field⁹. The inset in Fig. 4 shows a close-up of the noise measurement near 1 kHz, where spurious peaks can readily be identified. The peaks at 1 and 1.5 kHz are due to the spurious second and third harmonics of the 500 Hz excitation from our waveform generator. The peak at 1.175 kHz arises from the magnet stabilization system attached to our external magnet.

We remark here on practical considerations when using SKIFFS for magnetometry and other applications. First, the abrupt jumps shown in Fig. 2b limit the dynamic range of the device. The largest magnetic field that can be applied before an abrupt jump in the resonance frequency is a function of the geometry of the superconducting loop. The dynamic range can be extended by increasing the width of the nanowires. However, this choice comes at the expense of a loss in sensitivity, as wider nanowires reduce the kinetic inductance non-linearity of the loop²¹. In order to compensate for the reduced sensitivity, the loop area can be increased. Second, the operation of SKIFFS can be extended to even higher background magnetic fields by appropriately designing the superconducting loop parameters. For our thin-film, we estimate a zero-field London penetration depth of 450 nm. By choosing parameters for the superconducting loop that are smaller than the penetration

depth, the magnetic field resilience can be extended². Superconductors with large ($> 1 \mu\text{m}$) London penetration depths such as granular aluminum³⁶ may extend the use of SKIFFS to higher magnetic fields. Third, we have demonstrated readout of the microwave phase transmission through the SKIFFS devices. The detection sensitivity of the phase transmission is linearly dependent on the quality factor of the resonator. As a result, higher detection sensitivity can be achieved by ensuring that the loaded quality factor of the resonators remains high. For our devices, higher loaded quality factors can be achieved by adjusting the parameters of the coupling capacitor. Further improvement should be possible by operating at temperatures $T/T_C \ll 0.1$, where losses due to thermally excited quasiparticles and thermally activated motion of trapped flux vortices are significantly reduced. Finally, we note that even though we have applied small magnetic fields using a home-made coil, similar results can be obtained by driving DC currents through the central microwave feedline such that magnetic fields due to the currents couple into the SKIFFS loop. This provides a method of biasing SKIFFS on-chip, similar to the bias lines used for traditional SQUIDS.

The ability to detect small magnetic fields in the presence of large background fields provides a useful tool for several areas of research. For example, in the field of quantum computation, previous work has shown that small magnetic field fluctuations can lead to loss of quantum control of electron spins of donors in silicon as well as trapped ions on timescales longer than few milliseconds due to undesirable fluctuations in the background magnetic fields that provide the Zeeman splittings which are necessary for the experiments^{31,32,37}. In these settings, SKIFFS can be used to monitor the background magnetic fields and compensate for fluctuations. One approach is to build a magnetic-field-locked microwave source. In this application, the microwaves transmitted through a SKIFFS resonator can be used to drive spin rotations by appropriate frequency conversion through a phase-locked loop. More generally, SKIFFS can be used as resonators that can be tuned using magnetic fields instead of DC currents, and similar structures have been demonstrated for resonators which are capacitively coupled to a microwave feedline²⁵.

In summary, we have demonstrated the use of superconducting kinetic inductance field-frequency sensors for magnetometry in the presence of moderate background magnetic fields. We obtained resonance frequency shifts of 27 MHz in response to changes in magnetic field of $1.8 \mu\text{T}$. Real-time measurement of AC magnetic fields can be implemented by using phase-sensitive readout of microwaves transmitted through the sensors with a sensitivity of 1 degree/nT. We find that our sensors are at most one to two orders less sensitive in comparison with low-temperature superconducting quantum interference devices operating in zero background field. We anticipate potential applications of our sensors wherever small changes in a large background field must be accurately

monitored.

See supplementary material for a detailed derivation of Eq. 2 and estimates of the loop inductance and sensitivity of our devices.

We acknowledge helpful discussions with Shyam Shankar. Devices were designed using the CNST nanolithography toolbox³⁸ and fabricated in the Princeton Institute for the Science and Technology of Materials Micro/Nano Fabrication Laboratory and the Princeton University Quantum Device Nanofabrication Laboratory. Our work was supported by the NSF, in part through Grant No. DMR-1506862, and in part through the Princeton MRSEC (Grant No. DMR-1420541).

- ¹A. J. Annunziata, D. F. Santavicca, L. Frunzio, G. Catelani, M. J. Rooks, A. Frydman, and D. E. Prober, *Nanotechnology* **21**, 445202 (2010).
- ²N. Samkharadze, A. Bruno, P. Scarlino, G. Zheng, D. DiVincenzo, L. DiCarlo, and L. Vandersypen, *Phys. Rev. Applied* **5**, 044004 (2016).
- ³B. A. Mazin, *Microwave kinetic inductance detectors*, Ph.D. thesis, California Institute of Technology (2005).
- ⁴P. Szypryt, B. A. Mazin, B. Bumble, H. G. Leduc, and L. Baker, *IEEE Transactions on Applied Superconductivity* **25**, 1 (2015).
- ⁵J. Zmuidzinas, *Annu. Rev. Condens. Matter Phys.* **3**, 169 (2012).
- ⁶C. M. Natarajan, M. G. Tanner, and R. H. Hadfield, *Supercond. Sci. Technol.* **25**, 063001 (2012).
- ⁷A. N. McCaughan, *Superconducting thin film nanoelectronics*, Ph.D. thesis, Massachusetts Institute of Technology (2015).
- ⁸A. Kher, P. K. Day, B. H. Eom, J. Zmuidzinas, and H. G. Leduc, *J. Low Temp. Phys.* **184**, 480 (2016).
- ⁹J. Luomahaara, V. Vesterinen, L. Grönberg, and J. Hassel, *Nat. Commun.* **5**, 4872 (2014).
- ¹⁰B. Ho Eom, P. K. Day, H. G. LeDuc, and J. Zmuidzinas, *Nature Phys.* **8**, 623 (2012).
- ¹¹C. Bockstiegel, J. Gao, M. R. Vissers, M. Sandberg, S. Chaudhuri, A. Sanders, L. R. Vale, K. D. Irwin, and D. P. Pappas, *J. Low Temp. Phys.* **176**, 476 (2014).
- ¹²R. Erickson, M. Vissers, M. Sandberg, S. Jefferts, and D. Pappas, *Phys. Rev. Lett.* **113**, 187002 (2014).
- ¹³T. M. Hazard, A. Gyenis, A. Di Paolo, A. T. Asfaw, S. A. Lyon, A. Blais, and A. A. Houck, arXiv:1805.00938 [cond-mat, physics:quant-ph] (2018), arXiv: 1805.00938.
- ¹⁴J. T. Peltonen, P. C. J. J. Coumou, Z. H. Peng, T. M. Klapwijk, J. S. Tsai, and O. V. Astafiev, *Scientific Reports* **8**, 10033 (2018).
- ¹⁵STAR Cryoelectronics, LLC.
- ¹⁶H. L. Hortensius, E. F. C. Driessen, T. M. Klapwijk, K. K. Berggren, and J. R. Clem, *Appl. Phys. Lett.* **100**, 182602 (2012), <http://dx.doi.org/10.1063/1.4711217>.
- ¹⁷J. R. Clem and K. K. Berggren, *Phys. Rev. B* **84**, 174510 (2011).
- ¹⁸Sonnet Software Inc., <http://www.sonnetsoftware.com/>.
- ¹⁹B. Abdo, E. Segev, O. Shtempluck, and E. Buks, *J. Phys.: Conf. Ser.* **43**, 1346 (2006).
- ²⁰L. J. Swenson, P. K. Day, B. H. Eom, H. G. Leduc, N. Llombart, C. M. McKenney, O. Noroozian, and J. Zmuidzinas, *J. Appl. Phys.* **113**, 104501 (2013).
- ²¹A. T. Asfaw, A. J. Sigillito, A. M. Tyryshkin, T. Schenkel, and S. A. Lyon, *Appl. Phys. Lett.* **111**, 032601 (2017).
- ²²M. R. Vissers, J. Hubmayr, M. Sandberg, S. Chaudhuri, C. Bockstiegel, and J. Gao, *Appl. Phys. Lett.* **107**, 062601 (2015).
- ²³A. A. Adamyan, S. E. Kubatkin, and A. V. Danilov, *Appl. Phys. Lett.* **108**, 172601 (2016).
- ²⁴M. Tinkham, *Introduction to Superconductivity*, Dover Books on Physics Series (Dover Publications, 1996).
- ²⁵O. W. Kennedy, J. Burnett, J. C. Fenton, N. G. N. Constantino, P. A. Warburton, J. J. L. Morton, and E. Dupont-Ferrier, arXiv:1807.00582 [cond-mat, physics:physics] (2018), arXiv: 1807.00582.
- ²⁶M. J. Biercuk, A. C. Doherty, and H. Uys, *J. Phys. B: At. Mol. Opt. Phys.* **44**, 154002 (2011).
- ²⁷J. Bylander, S. Gustavsson, F. Yan, F. Yoshihara, K. Harrabi, G. Fitch, D. G. Cory, Y. Nakamura, J.-S. Tsai, and W. D. Oliver, *Nat Phys* **7**, 565 (2011).
- ²⁸M. Biercuk, H. Uys, A. VanDevender, N. Shiga, W. Itano, and J. Bollinger, *Phys. Rev. A* **79**, 062324 (2009).
- ²⁹J. T. Muhonen, J. P. Dehollain, A. Laucht, F. E. Hudson, R. Kalra, T. Sekiguchi, K. M. Itoh, D. N. Jamieson, J. C. McCallum, A. S. Dzurak, and A. Morello, *Nat Nano* **9**, 986 (2014).
- ³⁰J. Clarke and A. I. Braginski, *The SQUID Handbook Fundamentals and Technology of SQUIDs and SQUID Systems*, Vol. 1 (Wiley-VCH, Weinheim, 2006).
- ³¹A. M. Tyryshkin, S. A. Lyon, A. V. Astashkin, and A. M. Rait-simring, *Phys. Rev. B* **68**, 193207 (2003).
- ³²A. M. Tyryshkin, J. J. L. Morton, S. C. Benjamin, A. Ardavan, G. A. D. Briggs, J. W. Ager, and S. A. Lyon, *J. Phys.: Condens. Matter* **18**, S783 (2006).
- ³³S. M. Anton, J. S. Birenbaum, S. R. O'Kelley, V. Bolkhovskiy, D. A. Braje, G. Fitch, M. Neeley, G. C. Hilton, H.-M. Cho, K. D. Irwin, F. C. Wellstood, W. D. Oliver, A. Shnirman, and J. Clarke, *Phys. Rev. Lett.* **110**, 147002 (2013).
- ³⁴R. H. Koch, D. P. DiVincenzo, and J. Clarke, *Phys. Rev. Lett.* **98**, 267003 (2007).
- ³⁵A. Kou, W. Smith, U. Vool, R. Brierley, H. Meier, L. Frunzio, S. Girvin, L. Glazman, and M. Devoret, *Phys. Rev. X* **7**, 031037 (2017).
- ³⁶H. Rotzinger, S. T. Skacel, M. Pfirmann, J. N. Voss, J. Mnzberg, S. Probst, P. Bushev, M. P. Weides, A. V. Ustinov, and J. E. Mooij, *Supercond. Sci. Technol.* **30**, 025002 (2017).
- ³⁷J. W. Britton, J. G. Bohnet, B. C. Sawyer, H. Uys, M. J. Biercuk, and J. J. Bollinger, *Phys. Rev. A* **93**, 062511 (2016).
- ³⁸K. Coimbatore Balram, D. A. Westly, M. I. Davanco, K. E. Grutter, Q. Li, T. Michels, C. H. Ray, R. J. Kasica, C. B. Wallin, I. J. Gilbert, B. A. Bryce, G. Simelgor, J. Topolancik, N. Lobontiu, Y. Liu, P. Neuzil, V. Svatos, K. A. Dill, N. A. Bertrand, M. Metzler, G. Lopez, D. Czaplowski, L. Ocola, K. A. Srinivasan, S. M. Stavis, V. A. Aksyuk, J. A. A. Liddle, S. Krylov, and R. R. Ilic, *Journal of Research of the National Institute of Standards and Technology* **121**, 464 (2016).
- ³⁹T. Van Duzer and C. Turner, *Principles of Superconductive Devices and Circuits*, Bibliyografya Ve Indeks (Prentice Hall, 1999).
- ⁴⁰J. Gao, *The physics of superconducting microwave resonators*, Ph.D. thesis, California Institute of Technology (2008).

Supplementary Information for SKIFFS: Superconducting Kinetic Inductance Field-Frequency Sensors for Sensitive Magnetometry in Moderate Background Magnetic Fields

1. Kinetic Inductance and Flux Quantization

We begin by noting that the general expression for the kinetic inductance, L_k , of a superconducting wire of length l and cross-sectional area A can be found by equating the total kinetic energy of the Cooper pairs with the standard expression for the energy stored in an inductor, in complete analogy with magnetic (geometric) inductance⁷:

$$\frac{1}{2}L_k i^2 = \frac{1}{2}L_k (n_s \cdot 2e \cdot v_s \cdot A)^2 = \frac{1}{2}(2m_e)v_s^2 \cdot (n_s \cdot A \cdot l) \quad (\text{S1})$$

with m_e the mass of an electron, n_s (v_s) the density (velocity) of Cooper pairs and e the electronic charge. Solving for L_k , we find

$$L_k = \Lambda \frac{l}{A} \quad (\text{S2})$$

where $\Lambda = m_e/2n_s e^2$.

The supercurrent i_{loop} flowing through a superconducting loop is related to the magnetic field \vec{B} through the area enclosed by the loop via the flux quantization condition^{24,39}

$$\oint_C \Lambda \vec{J}_s \cdot \vec{dl} + \int_s \vec{B} \cdot \vec{ds} = n\Phi_0 \quad (\text{S3})$$

where J_s is the supercurrent density. Here, Φ_0 is the magnetic flux quantum, and the integrals are taken around the superconducting loop. We note that n can take on integer values.

2. Theory of Device Operation

For our particular devices, there are four sections within the superconducting loop as described in the main text: two nanowires on either side and two micron-sized wires completing the loop.

The first integral in Eq. S3 can be evaluated by considering the different sections of the superconducting loop separately. Denoting the loop current as i_{loop} , we write

$$\oint_C \Lambda \vec{J}_s \cdot \vec{dl} = \sum_{\text{sections}} \Lambda \frac{i_{\text{loop}}}{A_{\text{section}}} \cdot l_{\text{section}} \quad (\text{S4})$$

where the sum runs over each section of length l_{section} with cross-sectional area A_{section} . Using Eq. S2, the first integral in S3 reduces to

$$\oint_C \Lambda \vec{J}_s \cdot \vec{dl} = 2i_{\text{loop}} (L_{k_{\text{nano}}} + L_{k_{\text{micro}}}) \quad (\text{S5})$$

where $L_{k_{\text{nano}}}$ ($L_{k_{\text{micro}}}$) is the kinetic inductance of each nanowire (micron-sized) section of the loop. Here, we have assumed that the two nanowire sections are identical.

Next, we evaluate the second integral in Eq. S3. Given the area of the superconducting loop, A_{loop} , and assuming that the applied field is perpendicular to the loop, the total magnetic flux through the loop is the sum of the flux due to the externally applied magnetic field, $\Phi_{\text{ext}} = -BA_{\text{loop}}$, and the flux due to the screening current generated by the superconductor in response to the applied field, $\Phi_{\text{resp}} = L_{\text{geom}}i_{\text{loop}}$ where L_{geom} is the geometric portion of the total loop inductance. Here, the negative sign indicates that the screening flux opposes the externally applied flux. Writing L_{geom} as the sum of the geometric inductances of the nanowire and micron-sized sections, $L_{g_{\text{nano}}}$ and $L_{g_{\text{micro}}}$, respectively,

$$L_{\text{geom}} = 2(L_{g_{\text{nano}}} + L_{g_{\text{micro}}}) \quad (\text{S6})$$

Hence, the second integral in Eq. S3 becomes

$$\int_s \vec{B} \cdot \vec{ds} = -BA_{\text{loop}} + 2i_{\text{loop}}(L_{g_{\text{nano}}} + L_{g_{\text{micro}}}) \quad (\text{S7})$$

Combining Eqs. S5 and S7, the flux quantization condition in Eq. S3 becomes

$$i_{\text{loop}}L_{T_{\text{loop}}} - BA_{\text{loop}} = n\Phi_0 \quad (\text{S8})$$

where $L_{T_{\text{loop}}} = 2(L_{k_{\text{nano}}} + L_{g_{\text{nano}}} + L_{k_{\text{micro}}} + L_{g_{\text{micro}}})$ is the total loop inductance.

3. Estimating Resonance Frequencies from the Thin Film Parameters

We estimate the resonance frequency of each sensor as follows. From the sheet resistivity of the thin film ($252 \Omega/\square$), and the critical temperature ($T_C \sim 9 \text{ K}$), we estimate a sheet inductance of $L_s = 36 \text{ pH}/\square$ and a zero-field London penetration depth of 450 nm ^{5,24,40}. From the sheet inductance, we estimate that the nanowire section of the loop has a kinetic inductance of $360 \text{ pH}/\mu\text{m}$ while the $5 \mu\text{m}$ -wide section of the loop has a kinetic inductance of $7.2 \text{ pH}/\mu\text{m}$. From the total area of our loop ($\sim 100 \mu\text{m} \times 100 \mu\text{m}$) and for a $\ell_{\text{nw}} = 10 \mu\text{m}$ -long section of the nanowire, we estimate the total loop inductance to be $\sim 10 \text{ nH}$. Simulations using Sonnet software¹⁸ estimate the capacitance of the interdigitated structure at the center of the loop with $1 \mu\text{m}$ fingers and gaps to be 0.2 pF , leading to an estimated resonance frequency, $f_R = \frac{1}{2\pi} \sqrt{\frac{2}{10 \text{ nH} \times 0.2 \text{ pF}}} = 5.03 \text{ GHz}$. The factor of 2 comes from the parallel contribution of the left and right arms of the loop to the total loop inductance. The estimated resonance frequency is in reasonable agreement with the experimentally measured value of 4.182 GHz . A more accurate estimate requires accounting for the contribution of the $10 \mu\text{m}$ long tapers in the superconducting loop to the total kinetic inductance.

4. Estimating the Detection Sensitivity of Phase Readout

Assuming a phase change of π radians in 7 MHz for a resonance centered at 4 GHz with a quality factor of 600, the slope of the phase transmission through the res-

onance is ~ 30 degrees/MHz. In the main text, we have discussed that the resonators were biased such that the field-frequency conversion factor is 31 MHz/ μ T. Combining these two values, we estimate the detection sensitivity of phase readout to be 0.9 degrees/nT. This estimate is in good agreement with the experimentally observed sensitivity of 1 degree/nT.